Supporting Information

High Performance Broadband Photoelectrochemical Photodetectors Based on Cu-doped Bi_2O_2Se Nanosheets

Xinyu Guo, Yaning Hu, Jiaxing Wang, Ziyang Zhou, Peijie Ma*, Kun Zheng

State Key Laboratory of Materials Low-Carbon Recycling, Beijing University of Technology, Beijing 100124, China.

During thesynthesis, there were four potential chemical reactions:

$Bi(NH_3)_2C_6H_7O_7 \rightarrow Bi^{3+} + 2NH_4^+ + C_6H_5O_7^{3-}$

$CuCl_2 \rightarrow Cu^{2+} + 2Cl^-$

$Bi^{3+} + NH_4^+ + C_6H_5O_7^{3-} + 4KOH \rightarrow Bi(OH)_4NH_4 + K_3C_6H_5O_7 + K^+$

$Bi(OH)_4NH_4 + Na_2SeO_3 + xCu^{2+} \rightarrow Bi_{2-x}Cu_xO_2Se + N_2 + NaOH + H_2O$

Table S1 The power intensities of various wavelengths of light

P(Mw/cm^2) / Light(nm)	I	II	III	IV
365	1.3	3.39	5.78	10.68
400	1.55	3.08	5.77	8.68
500	3.64	5.04	10.8	13.87
600	3.2	5.92	8.58	14.5
700	2.8	4.91	10.06	15.77

Table S2 The photocurrent density of CBOS PEC photodetectors for various wavelengths of light with different power intensities under 0V

I(μA/cm^2) / Light(nm)	I	II	III	IV
365	0.724	1.384	1.992	3.62
400	0.48	0.92	1.64	2.28
500	0.36	0.44	0.88	1.08
600	0.32	0.56	0.80	1.32
700	0.24	0.28	0.56	0.64

Table S3 The responsivity of CBOS PEC photodetectors for various wavelengths of light with different power intensities under 0V

R(mA/W) / Light(nm)	I	II	III	IV
365	0.55	0.408	0.344	0.338
400	0.310	0.200	0.300	0.260
500	0.098	0.087	0.081	0.077
600	0.100	0.095	0.093	0.091
700	0.086	0.057	0.055	0.046

Table S4 The photocurrent density of CBOS PEC photodetectors under 365nm light illumination with different power intensities and different bias voltages

I(μA/cm^2) / Bias(V)	I	II	III	IV
0	0.724	1.384	1.992	3.62
0.2	1.198	2.061	3.328	6.100
0.4	2.892	3.604	6.008	10.296
0.6	14.008	16.832	19.744	28.456

Table S5 The responsivity of CBOS PEC photodetectors under 365nm light illumination with different power intensities and different bias voltages

R(mA/W) / Bias(V)	I	II	III	IV
0	0.55	0.408	0.344	0.338
0.2	0.92	0.61	0.344	0.57
0.4	2.23	1.06	1.03	0.964
0.6	10.778	4.97	3.42	2.66

Table S6 Comparison of Photoelectric Properties in Hydrothermally Synthesized 2D Materials

	R(mA/W)	Raise/decay(s)	Refs.
CBOS	10.78	0.06/0.06	This work
SnS_2	1.46	0.32/1.15	(1)
SnSe	0.00005	0.17/0.51	(2)
Bi_2O_2Se	0.02	0.2/0.12	(3)
CuO	2.7	0.06/0.4	(4)
ZnO/MoS_2	4	0.15/0.17	(5)
Te/Se	0.083	0.14/0.47	(6)

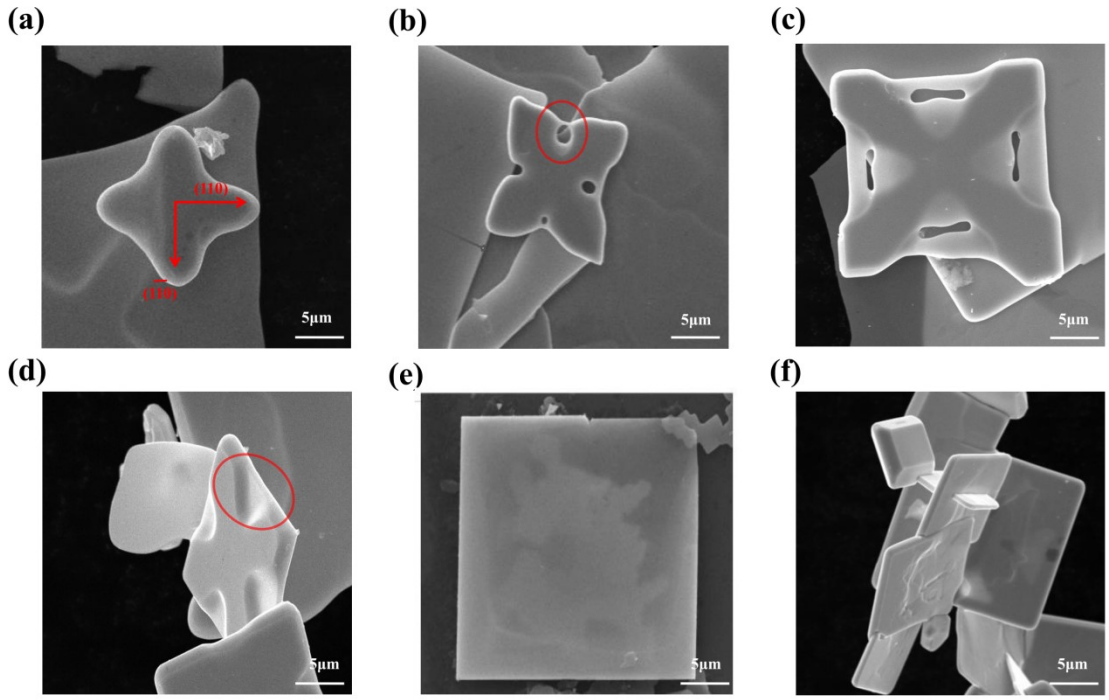

Figure S1 SEM image (a-f) present the formation process of Cu-doped Bi_2O_2Se square nanosheets.

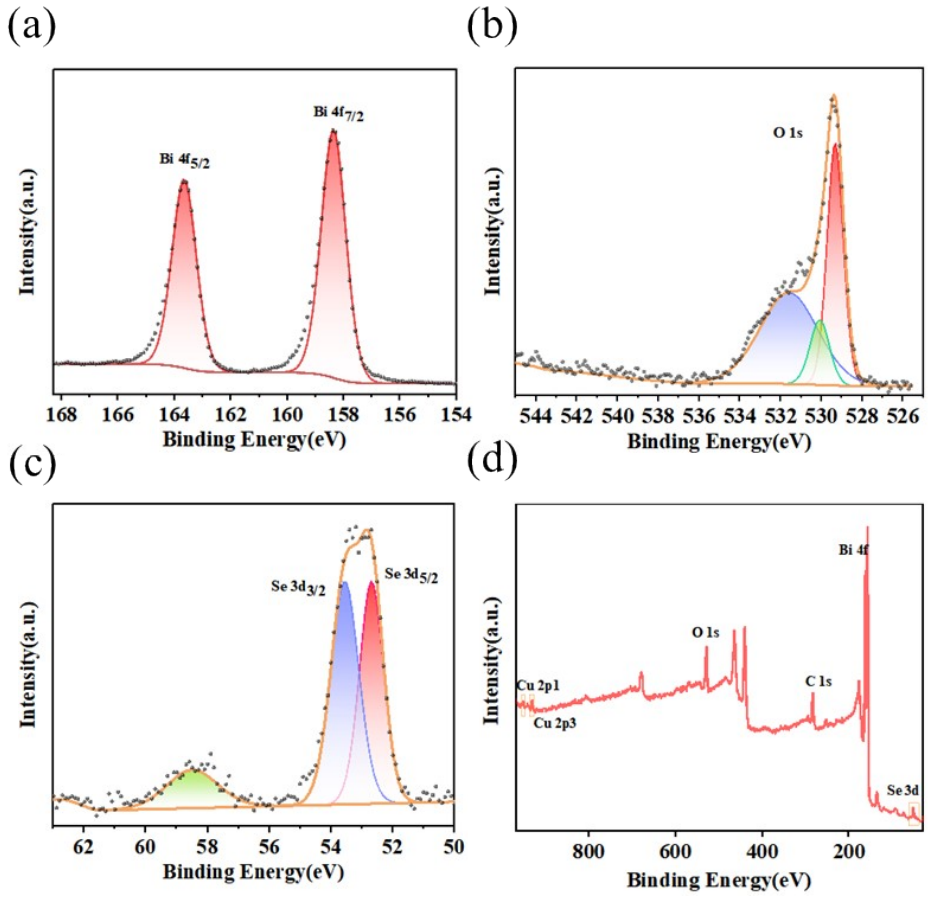

Figure S2 XPS spectra. (a) present the full-scale XPS scan of the 2D CBOS nanosheets. (b-c) present XPS spectra of Cu, Bi, O, and Se, respectively.

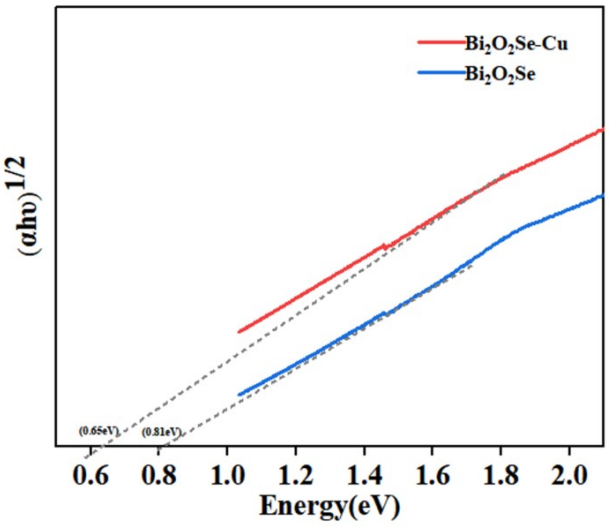

Figure S3 Comparative plot of Tauc curves for Bi_2O_2Se and Cu-doping Bi_2O_2Se.

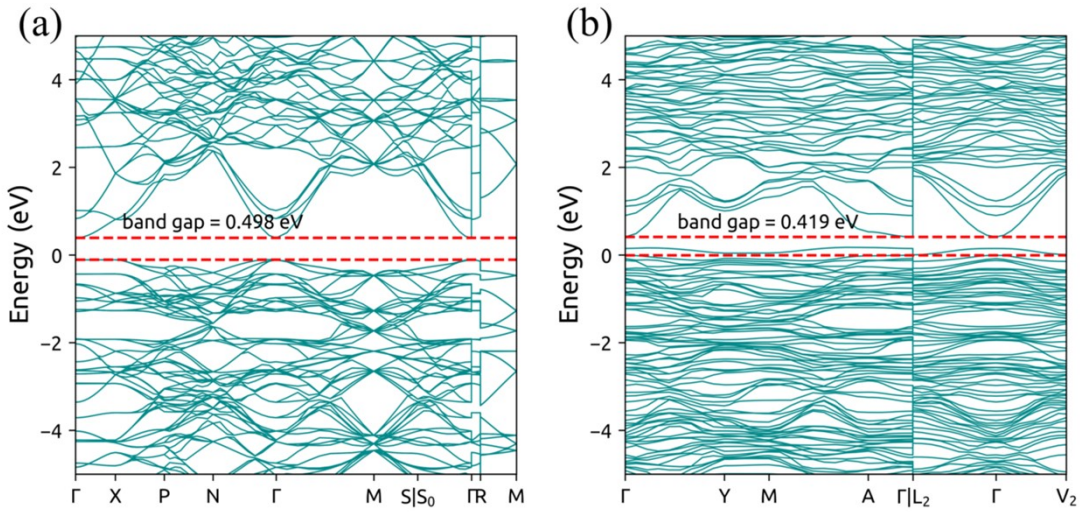

Figure S4. DFT-calculated band structures of Bi_2O_2Se before and after Cu doping. (a) Intrinsic Bi_2O_2Se with a band gap of 0.498 eV. (b) Cu-doped Bi_2O_2Se (CBOS) with a narrowed band gap of 0.419 eV, showing a marked upward shift of the valence band maximum.

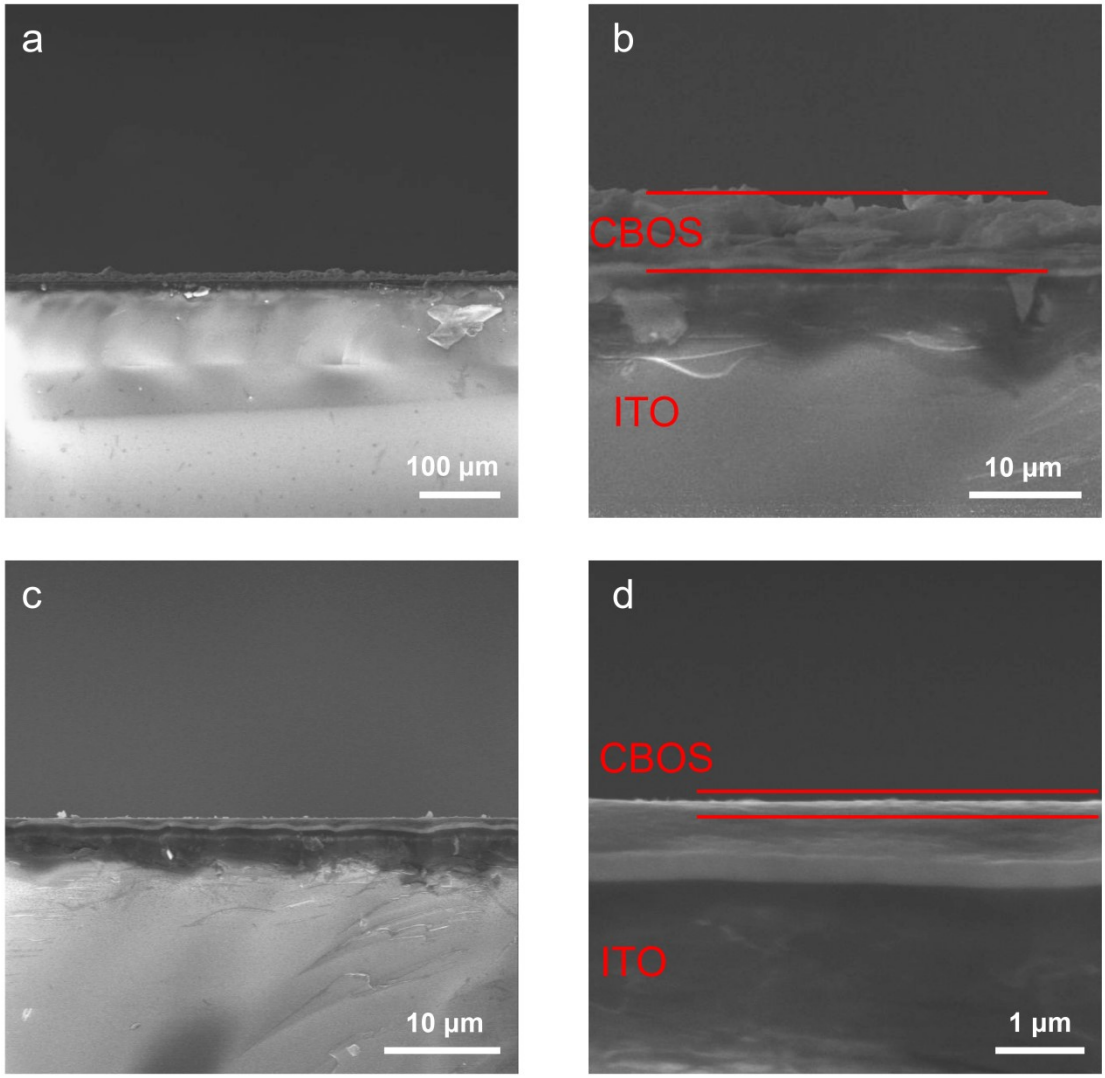

Figure S5. Cross-sectional SEM characterization of CBOS films on ITO substrates prepared from solutions with different concentrations.(a, b) Low-magnification (a) and high-magnification (b) cross-sectional views of a high-concentration CBOS film. The red outlines highlight the uniformly coated CBOS layer. (c, d) Low-magnification (c) and high-magnification (d) cross-sectional views of a low-concentration CBOS film.

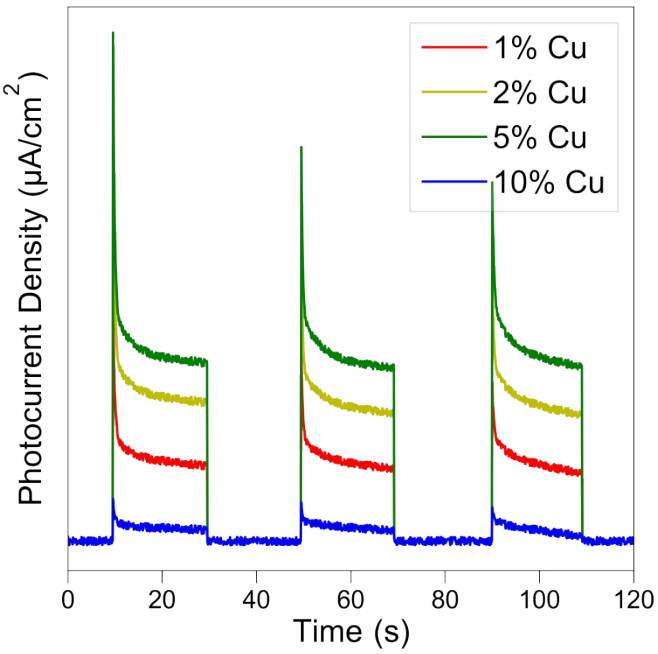

Figure S6. Photocurrent density versus time curves for samples with different feeding Cu/Bi ratios

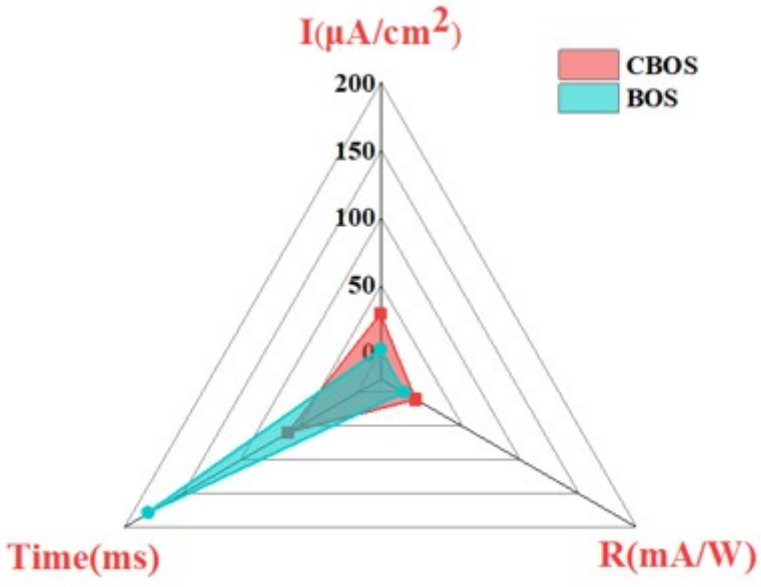

Figure S7 Performance Comparison Chart of BOS and CBOS

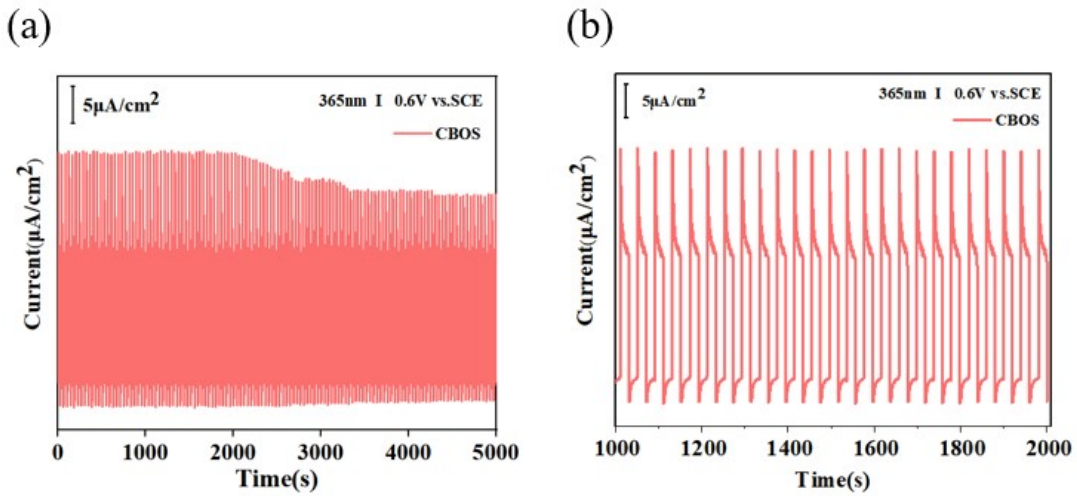

Figure S8 Stability of the 2D CBOS photodetector. (a) Long-term stability tests of the 2D CBOS PEC photodetector for 5000 s illuminated by 365nm (level I) at 0V. (b) 25 cycles intercepted from 1000-2000s

Reference

(1) Deng, S., Chen, Y., Li, Q., Sun, J., Lei, Z., Hu, P., ... & Ma, R. Direct growth of SnS_2 nanowall photoanode for high responsivity self-powered photodetectors. *Nanoscale* **2022**, *14*(38), 14097-14105.

(2) Liang, Z., Hao, R., Luo, H., He, Z., Su, L., & Fan, X. Enhancing the photo-response performance of a SnSe-based photoelectrochemical photodetector via Ga doping. *Journal of Materials Chemistry C* **2024,** *12*(8), 2981-2992.

(3) Chen, G., Wu, J., Wang, B., Li, J., & Qi, X. High-performance self-powered photodetector based on Bi_2O_2Se nanosheets. *Applied Physics A* **2020**, *126*(7), 579.

(4) Gao, Q., Jin, Z., Qu, L., Shao, Z., Liu, X., Zhang, Y., ... & Feng, W. CuO nanosheets for use in photoelectrochemical photodetectors. *ACS Applied Nano Materials* **2022**, *6*(1), 784-791.

(5) Ma, J., Ge, Y., Dai, P., Lu, C., & Xu, X. Highly stable and sensitive photoelectrochemical photodetectors based on a ZnO nanorod/monolayer MoS_2 nanosheets heterostructure. *Journal of Alloys and Compounds* **2024**, *976*, 173315.

(6) Wang, Y., Zhao, F., Wang, Y., Zhang, Y., Shen, Y., Feng, Y., & Feng, W. Broadband self-powered photoelectrochemical photodetector based on Te/Se heterostructure nanocomposites. *Composites Communications* **2022**, *32*, 101175.